Journal of Sound and Vibration (1999) **228**(3), 459–475
Article No. jsvi.1998.2418, available online at http://www.idealibrary.com on IDEAL®

NUMERICAL SIMULATION OF LAMINAR FLOW PAST A TRANSVERSELY VIBRATING CIRCULAR CYLINDER

B. S. VARAPRASAD PATNAIK* AND P. A. ASWATHA NARAYANA
Department of Applied Mechanics, IIT, Madras 600 036, *India*

AND

K. N. SEETHARAMU
Department of Mechanical Engineering, IIT, Madras 600 036, *India*

(*Received* 7 *October* 1997 *and in final form* 21 *December*, 1998)

Flow past a transversely vibrating circular cylinder is numerically simulated by solving the Navier–Stokes equations and by implementing a modified velocity correction method. Galerkin weighted residual formulation is employed for the spatial discretization along with a second order Runge–Kutta time integration. Primitive variables are approximated by polynomial basis functions defined over three-noded linear triangular elements. The frame of reference is fixed with respect to the vibrating body and the additional acceleration term arising out of this non-inertial transformation is added to the Y-momentum equation. The influence of the cylinder vibration on the wake patterns, phase plane, lift and drag forces, etc., is investigated. The synchronization regime or the "lock-in" boundaries are also established from the present numerical simulations.

1. INTRODUCTION

It is well known that vortices are formed and shed in the wakes of bluff bodies over a wide range of Reynolds numbers. When a circular cylinder is subjected to vibration, its amplitude and frequency influence the wake patterns in the downstream. This classical and practically relevant phenomenon has its applications on a number of engineering design parameters connected with fluid flow, heat transfer and vibration. Applications abound in heat exchanger tubes, nuclear reactor fuel rods, cooling towers, chimney-stacks, offshore structures, etc. Apart from the engineering relevance, a study of these mechanisms associated with the laminar flow past cylinders, forms the first step towards understanding the vastly more complicated phenomenon of turbulence [1] and also towards understanding more complex systems [2]. A deeper insight into the associated mechanisms will help the designers on the active control of vortex shedding. Hence, a computer program for the prediction of flow past a vibrating structure would be invaluable in engineering analysis and design.

* Present address: Department of Mechanical Engineering, UBC, Vancouver, Canada V6T 1Z4.

0022-460X/99/480459 + 17 $30.00/0

When the forcing frequency is in the neighborhood of the natural vortex shedding frequency (the latter is also known as the Strouhal frequency), the response of the forced wake is such that, it synchronizes with the forcing frequency for certain amplitudes of vibration [3]. Koopman [4] has also investigated the effect of the forced transverse oscillations of a circular cylinder. The study, however, has focussed on obtaining the "lock-in" boundary.

The first successful attempt to numerically simulate the flow past a vibrating body was by Hurlbut *et al.* [5], which employed the popular marker and cell (MAC) finite difference method. Further, Chilukuri [2] applied simplified marker and cell (SMAC) method to achieve this objective. Li *et al.* [6] and Sun *et al.* [7] employed a periodic parietal velocity forcing on a quiescent cylinder to simulate the flow past an oscillating body. Further, it was pointed out that, such an approximation was limited by the amplitude ratio of cylinder excitation ($a/d < 0{\cdot}2$). However, in these studies, an analysis of the wake patterns was not attempted. Recently, Meneghini and Bearman [8] have used a discrete vortex method (DVM) with a vortex-in-cell (VIC) procedure, by incorporating viscous diffusion. As this method employs streamfunction–vorticity formulation, it cannot be extended to three dimensions. Wei *et al.* [9] have used a promising approach of remeshing only a part of the domain around the oscillating body by an arbitrary Lagrangian Eulerian (ALE) approach. However, their time-dependent remeshing technique is computationally more involved.

In the present study, a different approach of analyzing the wake patterns is applied by employing a primitive variable formulation. The Runge–Kutta (R–K) time integration scheme, along with a Galerkin-weighted residual formulation for spatial discretization, are implemented to solve the Navier–Stokes equations. As the reference frame is fixed with respect to the vibrating body, an additional acceleration term arising out of this non-inertial transformation is added to the Y-momentum equation. An analysis of the wake is carried out with a simple and novel Lagrangian method, termed numerical particle release (NPR). The temporal lift and drag coefficients are obtained. The boundary region for "synchronization" is also captured.

2. GOVERNING EQUATIONS AND BOUNDARY CONDITIONS

The time-dependent Navier–Stokes and continuity equations, applicable for two-dimensional, laminar, incompressible flows, after the following non-dimensionalization,

$$x = X/D, \qquad y = Y/D; \qquad u = U/U_\infty, \qquad v = V/U_\infty,$$
$$\tau = t^* U_\infty/D, \qquad p = P_\infty/\rho U_\infty^2 \tag{1}$$

are given by equations (2)–(4). Here, D is the cylinder diameter, and U_∞ and P_∞ refer to the free stream velocity and pressure respectively,

$$\frac{\partial u}{\partial x} + \frac{\partial v}{\partial y} = 0, \tag{2}$$

$$\frac{\partial u}{\partial t} + u\frac{\partial u}{\partial x} + v\frac{\partial u}{\partial y} = -\frac{\partial p}{\partial x} + \frac{1}{Re}\nabla^2 u \tag{3}$$

$$\frac{\partial v}{\partial t} + u\frac{\partial v}{\partial x} + v\frac{\partial v}{\partial y} = -\frac{\partial p}{\partial y} + \frac{1}{Re}\nabla^2 v + \frac{\mathrm{d}^2 y}{\mathrm{d}t^2} \tag{4}$$

where $y = a\sin(2\pi f_e t)$ with f_e being the excitation frequency and a the amplitude of vibration.

To achieve the present objective, the frame of reference is fixed with respect to the vibrating cylinder. Such a non-inertial transformation results in an additional acceleration term in the Y-momentum equation. The in-flow boundary is specified with a superimposed oscillatory flow in the transverse direction over and above the free stream velocity (U_∞). The top and bottom boundaries are located at a distance of 10 times the cylinder diameter, where the free stream velocity is imposed. A no-slip boundary condition is satisfied on the cylinder surface. The down stream boundary is located such that it does not influence the vortices formed in the near wake of the cylinder. This is naturally incorporated and arises in the context of the finite element method, as applied to the Navier–Stokes equations. Hence, the outflow boundary condition is of the form

$$-p + \frac{1}{Re}\left(\frac{\partial U}{\partial X}\right) = 0{\cdot}0; \qquad \frac{1}{Re}\left(\frac{\partial V}{\partial Y}\right) = 0{\cdot}0.$$

Thus, a homogeneous Neumann boundary condition is naturally incorporated, with a traction-free exit. However, it should be mentioned that the above equations are implemented in a weak fashion rather than in a pointwise manner.

3. MATHEMATICAL FORMULATION

The algorithm employed in the present study is the modified velocity correction method (MVCM) of Ren and Utnes [10], which is essentially an extension of the popular projection scheme of Chorin [11]. In this scheme, the time integration is based on a Runge–Kutta (R–K) mid-point procedure; which is second-order-accurate. The spatial discretization is performed by the finite-element-based Galerkin-weighted residual formulation with linear triangular elements. The following four steps are repeated within each iteration.

(1) Calculation of Runge–Kutta coefficients (K_1, K_2) in order to obtain an intermediate velocity field ($\tilde{\mathbf{u}}$), by omitting the pressure and acceleration terms in equations (3) and (4):

$$K_1 = \Delta t\left(\frac{1}{Re}\nabla^2 u^n - (u^n\,\nabla)\,u^n\right), \tag{5}$$

$$u_k = u^n + K_1, \tag{6}$$

$$K_2 = \Delta t\left(\frac{1}{Re}\nabla^2 u_k - (u_k\,\nabla)\,u_k\right) \tag{7}$$

(2) Calculation of the intermediate velocity field ($\tilde{\mathbf{u}}$):

$$\tilde{\mathbf{u}} = (u^n) + \frac{K_1 + K_2}{2}. \tag{8}$$

(3) Solving for pressure from the Poisson equation:

$$\nabla^2 P^n = \frac{1}{\Delta t} (\nabla \cdot \tilde{\mathbf{u}}). \tag{9}$$

(4) Applying correction to the intermediate velocity field

$$\mathbf{u}^{n+1} = \tilde{\mathbf{u}} - \Delta t \, (\nabla \mathbf{P}^n - A) \tag{10}$$

where

$$\mathbf{u} = (u, v), \qquad A = \mathrm{d}^2 y / \mathrm{d}t^2.$$

Finite element spatial discretization is performed by the Galerkin-weighted residual formulation, where the shape function itself happens to be the weighting function. Linear triangular elements (with i, j, k as the subscripts) are used to represent u, v and p, which are approximated as

$$\begin{aligned} u &= N_i u_i + N_j u_j + N_k u_k, \\ v &= N_i v_i + N_j v_j + N_k v_k, \\ p &= N_i p_i + N_j p_j + N_k p_k. \end{aligned} \tag{11}$$

Global matrices are formed separately to solve for u, v and p. Specific details of the formulation are available in reference [12], and the shape functions, defined for the triangular elements are in reference [13]. The implementation methodology is elaborated in reference [14]. After obtaining the velocity field, the following stream function equation is solved with appropriate boundary conditions to obtain the ψ distribution of the flow field.

$$\frac{\partial^2 \psi}{\partial X^2} + \frac{\partial^2 \psi}{\partial Y^2} = -\left[\frac{\partial V}{\partial X} - \frac{\partial U}{\partial Y}\right].$$

In the present study, stability of the algorithm is limited by the advection–diffusion term in the equation for the velocity correction phase. Thus, the time step is governed by

$$C < \left\langle \frac{Pe}{2 + Pe} \right\rangle$$

where the Courant number $(C) = U(\mathrm{d}\tau/\mathrm{d}x)$ and the cell Peclet number $(Pe) = U \, \mathrm{d}x/v$.

Even though the absolute error is taken as the criterion for convergence, as the type of solution involved in the present simulation is "steady periodic" in nature, the iterative process ceases after obtaining about 25–30 vortex shedding cycles. It is well known that, the discretization process involves a certain amount of error, which can be systematically reduced in principle by a series of grid refinements.

Three types of mesh have been chosen for this purpose, to check for the self-consistency of the present study. These are:

(A) 1464 nodes; 2872 elements.

(B) 2124 nodes; 4298 elements.

(C) 2568 nodes; 5476 elements.

The results have shown a maximum difference of only about 1·5–2%, in the average centerline velocities, Strouhal numbers, Nusselt numbers, etc., between B and C type grids, while the variation between B and C type grids is about 5–6%. Thus, B type mesh density is found to be adequate, and hence is used in the subsequent simulations.

4. RESULTS AND DISCUSSION

4.1. FLOW PAST AN ISOLATED CIRCULAR CYLINDER

Flow past an isolated circular cylinder is simulated as a precursor to study the influence of cylinder vibration. Over a range of Reynolds numbers, extensive comparisons are made, with respect to a number of fluid flow parameters of interest in engineering design, such as the mean centerline velocities, Strouhal number, Nusselt number, lift and drag coefficients, etc. These comparisons are available in the investigations of Patnaik [14] and Patnaik *et al.* [15]. Velocity vectors for a typical case of natural vortex shedding are presented in Figure 1(a) and its corresponding streamline pattern in Figure 1(b). Here, the downstream wake region is sinuous in nature, while the upstream resembles like a potential flow. The velocity vectors of the domain indicate a fairly uniform profile at the exit boundary.

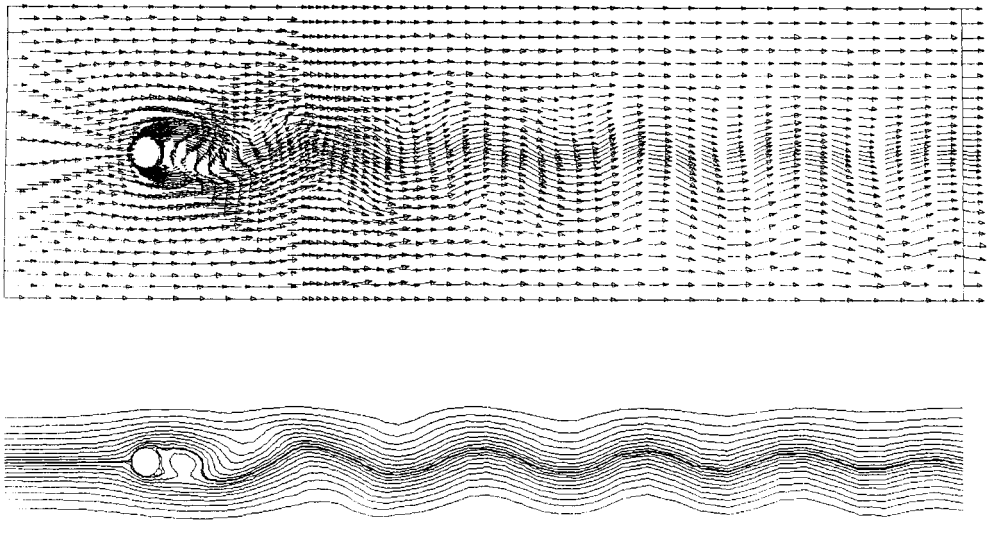

Figure 1. (a). Velocity vectors for flow past a circular cylinder, $Re = 80$. (b) Streamlines for flow past a circular cylinder, $Re = 80$.

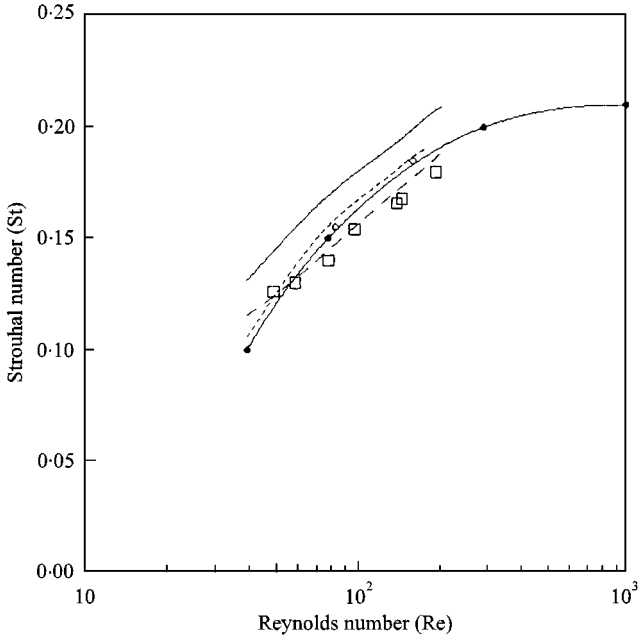

Figure 2. Strouhal number (St) against Reynolds number. —— Karniadakis [20]; - - - - Williamson [21]; – – – – Sa and Chang [22]; ○○○○○ Chilukuri [2], grid 2; ●●●●● Kovasznay [23]; □□□ Present study.

The time period of vortex shedding (T_{ps}) is obtained from the signal traces of the cross-stream component of velocity (U_y) along the axis of symmetry in the downstream region. About 12 nodal locations are monitored and their time histories are obtained. Strouhal number, which is a measure of the oscillating fluid flow phenomenon and is also the vortex shedding design parameter of interest, is plotted in Figure 2, over a range of Reynolds numbers. Natural vortex shedding frequency (f_{vs}) becomes identical with the Strouhal number (St), as they are bound by the relation ($St = f_{vs} D/U_\infty$), when both the cylinder diameter and the free stream velocity are rendered as unity. Temporal lift and drag coefficients are obtained by integrating the viscous and form drag contributions. A good comparison of the average drag coefficient with earlier investigations can be seen in Figure 3.

4.2. NUMERICAL PARTICLE RELEASES (NPR)

Streamlines are primarily flow lines which indicate the instantaneous flow pattern while path lines represent the locus of all such locations at which a specific particle was dwelling. However, the capability of either the streamlines or the path lines to project the spatio-temporal history of the wake is very much restricted. In the experimental flow visualization, in order to obtain the wake behaviour, various physical tracers such as hydrogen bubbles, tufts, oil films, smoke particles, dye, etc., are used. The major contribution of the present study lies in the implementation of

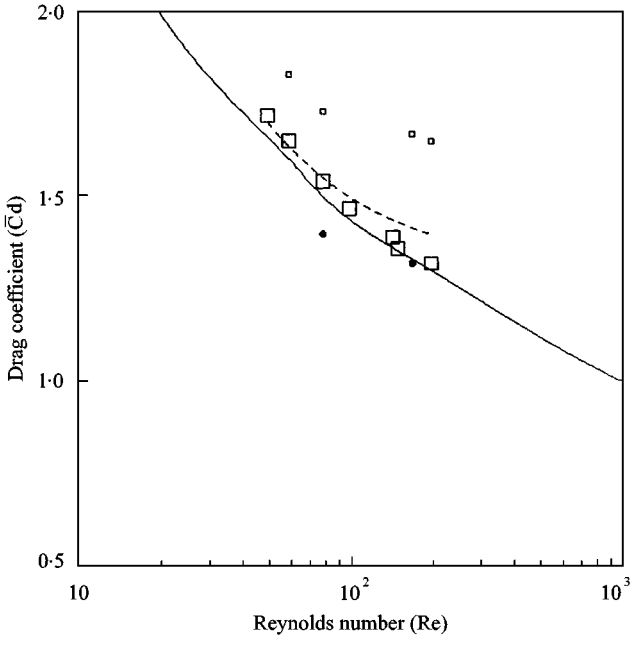

Figure 3. Comparison of drag coefficient ($\bar{C}_d$) with Reynolds number. —— Griffin and Votaw [24]; □□□□ Chilukuri [2], grid 1; ●●●●● Chilukuri [2], grid 2; - - - Karniadakis [20]; □ □ □ □ Present study.

a simple, and novel procedure for the particle release, termed numerical particle release (henceforth referred as NPR), to obtain the detailed structure of the downstream wake. NPR is devoid of the problem of the tracer getting diffused into the main flow, unlike in the experimental visualization. The particles are released in the near-wake region of the cylinder and from a number of distinct locations. A fine local control (i.e., desired interval and location) on the release of these particles was also incorporated. Particle releases are continuous in time and are updated with their current locations. A simple book-keeping procedure was adopted to reduce the "search time" involved in locating the new and updated positions of these particles. The search philosophy primarily involved the following steps: (1) search within the element, (2) search the neighbors of the element, (3) further, its neighbors and so on … The search is extended till the new position of the particle is identified. This novel search reduction strategy reduces an enormous amount of computing time. Interestingly, a specific particle, which is released earlier in time, can lag behind a particle released later in time, even if it is released from the same location. This is attributed to the history and transport effects associated with the vortex shedding process. However, the particle updating ceases when they cross the outflow boundary.

A typical streakline pattern thus obtained by NPR, is depicted in Figure 4, which represents the structure of the wake for a natural shedding case and for a Reynolds number of 100. The visual obtained from the present finite element simulation is compared with an experimental visual, in the same figure. In the

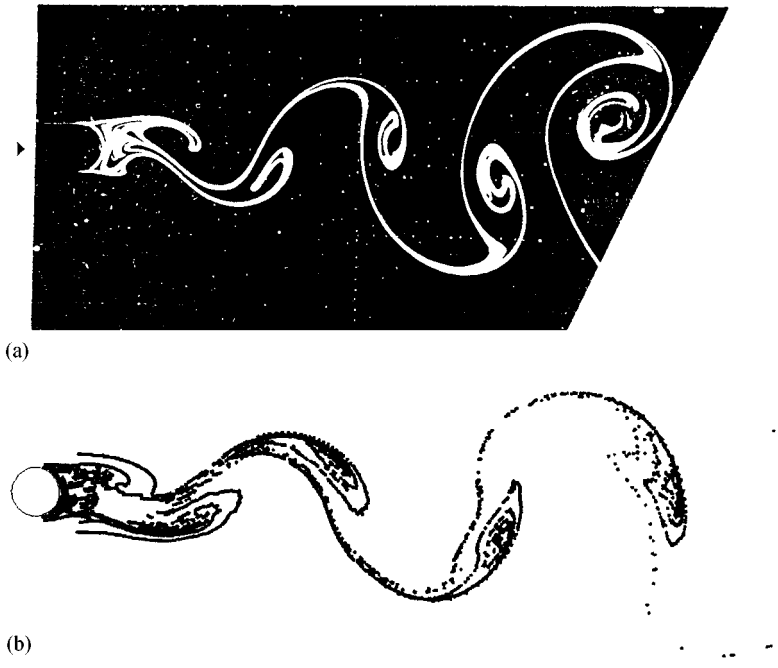

Figure 4. Comparison of streaklines with an experimental visual: (a) experimental visual [16]; (b) numerical visual.

experimental case [16], the Kármán vortex street behind the circular cylinder is made visible by means of an electrolytic precipitation method and the white curves are known as streaklines. The distinct feature of this comparison is the kind of similarity in the vortex trail and the gradual roll-up of shear layers at crests and troughs. All these eddies are mutually connected by the streaklines which originate in the near wake. The vortex pattern associated with the natural vortex shedding is very well represented in the numerical flow visual. By means of a number of schematics, Perry *et al.* [17] have shown that, every eddy shed is ultimately interconnected with every other eddy by its own "umbilical cord". This aspect can be clearly seen in the numerical and experimental visuals.

4.3. FLOW PAST A VIBRATING CIRCULAR CYLINDER

When a circular cylinder vibrates due to self-excitation or otherwise, an analysis of its wake becomes important. Also, the physics associated with the wake patterns can be better understood. Hence, simulations are carried out for various combinations of excitation frequencies (f_e/f_{ns}) between 0·6 and 1·4 (in steps of 0·1) and amplitudes of vibration ($a/d = 0{\cdot}05$, 0·14, 0·25), and over the low Reynolds number range. Some comparisons could be made with the available experimental investigations of Tanida *et al.* [18] for $Re = 80$.

4.3.1. *Lock-in boundary*

The type of response to a varying excitation frequency, and for different amplitudes of vibration, viz. $a/d = 0{\cdot}05$, $0{\cdot}14$ and $0{\cdot}25$, are analyzed to generate the "lock-in" boundary (also known as, "the synchronization regime"). Phase plane plot is a diagram plotted continuously in time between any two state vectors of a domain. The velocities along (U_x) and across (U_y) the stream serve this purpose in the present case. Their temporal histories are monitored at nodes located in the near wake of the cylinder. For the sake of brevity, only the influence of excitation frequency for a fixed amplitude of vibration (a/d) equal to $0{\cdot}14$ is plotted in Figure 5. Here, the phase plane can be seen in unstable periodic orbits for the cases, where $f_e/f_{ns} < 0{\cdot}8$. However, for $f_e/f_{ns} = 0{\cdot}8$, the departure of the chaotic phase plane into a single and stable periodic orbit can be noticed. This is popularly known as "limit-cycle". As can be observed in Figure 5, it persists up to $f_e/f_{ns} = 1{\cdot}2$, indicating that there exists a range over which the excitation frequency is able to drive the shedding frequency into its corresponding value. For $f_e/f_{ns} > 1{\cdot}2$, the phase plane again becomes aperiodic and chaotic. Further, the presence of these frequencies can also be explained from the fast fourier transforms (FFTs) taken from the lift coefficient histories, which are also depicted in the same figure. Here, the presence of a single unique peak indicates "lock-on", while the dominance of both the frequencies is called "non-lock-on". Even in the classical experiments of Koopman [4], a Lissajous figure was observed in order to judge, as to when the hot-wire signal and the driver oscillator were of the same frequency. The vortex street was considered to be "locked-in", when the Lisasjous figure appeared as a "steady single loop". In his experiments, vibration of the cylinder was started at the natural shedding frequency. After a fixed displacement for the amplitude was chosen, the driving frequency was slowly varied until a stable single pattern of Lissajous figure vanished, thus indicating that an end point has been reached.

A comparison of the "latch-on" frequency range is shown in Figure 6, which is compared with the experimental studies of Tanida *et al.* [18]. The present results compare well over most of the range, however, they underpredict the frequency range of the experiments. Similar "lock-in" frequency range is also determined for the other two amplitudes of vibration, viz. $a/d = 0{\cdot}05$ and $0{\cdot}25$. At $a/d = 0{\cdot}05$, the "lock-in" frequency range is found to be smaller, while it is broader at $a/d = 0{\cdot}25$. As a summary of these investigations, "lock-in" boundary is drawn and a good comparison of the same can be seen in Figure 7, with the available experimental and numerical investigations. Also depicted in the figure is the "no-lock-in" boundary, which is on the immediate outer side to the two "lock-in" curves. The work of Li *et al.* [6], which uses a parietal velocity forcing overestimates of the "lock-in" boundary, in comparison with the experimental observations of Koopman [4]. The present results are closer to the experimental investigations, as this study employed a more realistic simulation procedure combined with the choice of a good numerical scheme. Also depicted is the boundary curve given by Meneghini and Bearman [8], who have employed a discrete vortex method. As can be observed, the frequency range between the "lock-in" boundaries is wider at higher amplitudes and smaller at lower amplitudes of vibration.

Karniadakis and Triantfyllou [19] have characterized the state of both forced and unforced vortex wakes by means of a qualitative state diagram (similar to Figure 7). At small but finite amplitudes, the transitions corresponding to the upper

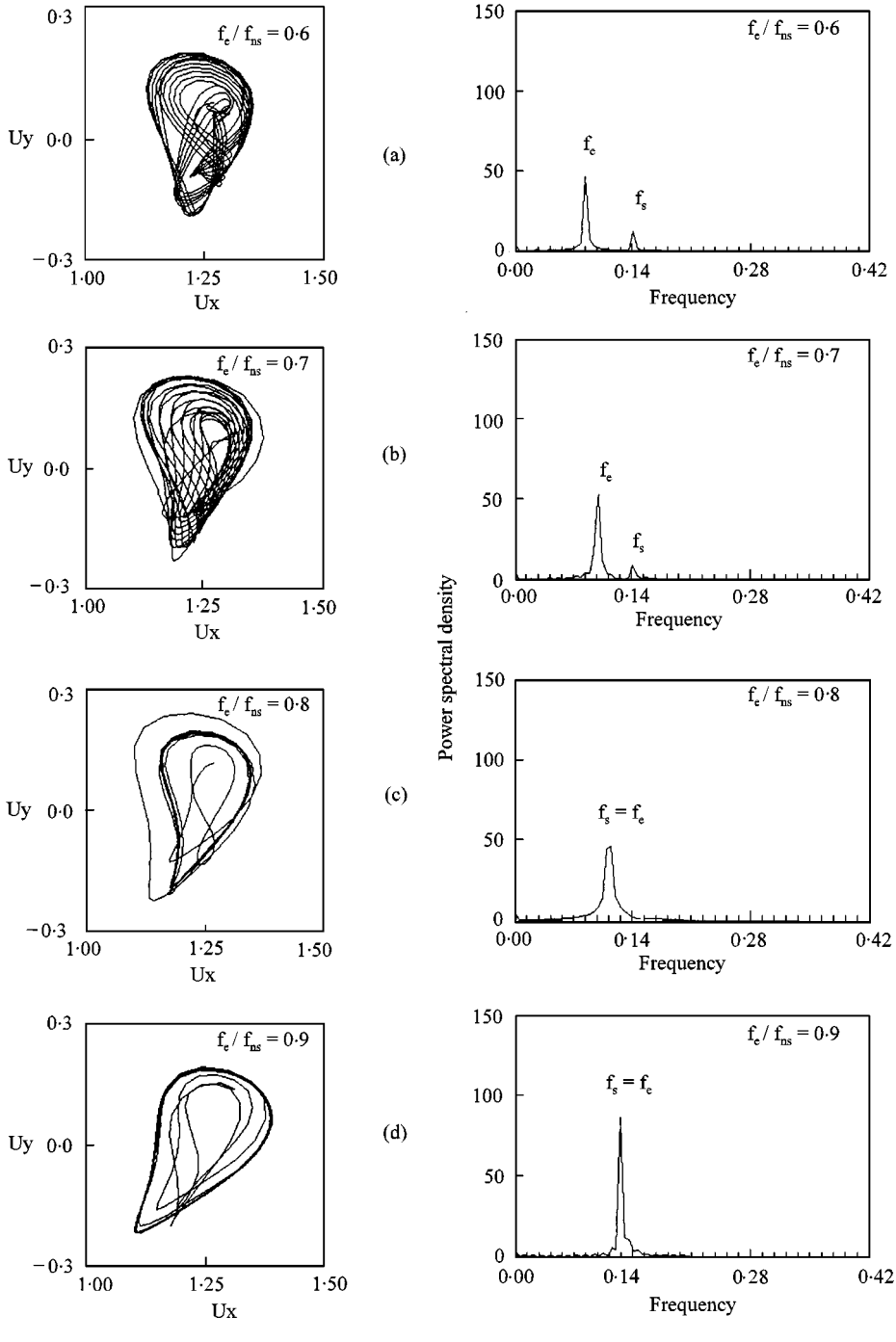

Figure 5. Phase plane and FFTs for a vibrating circular cylinder at $Re = 80$.

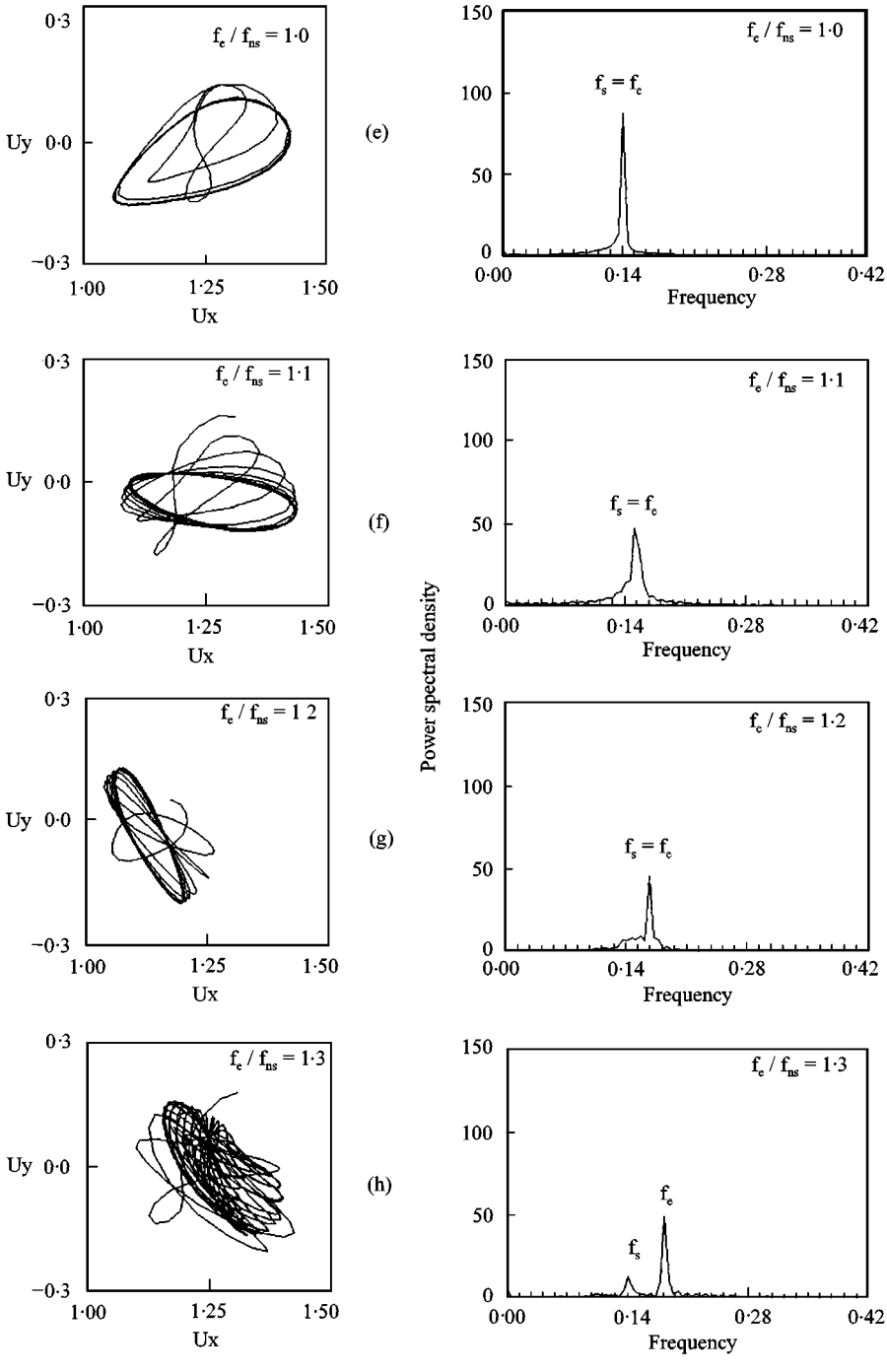

Figure 5. Continued.

and lower limits of "lock-on" are given by two bounding frequencies; within these limits only periodic lock-on states exist. In this investigation, quasi-periodic regions are thought to develop at frequencies well above and below the lock-on regime,

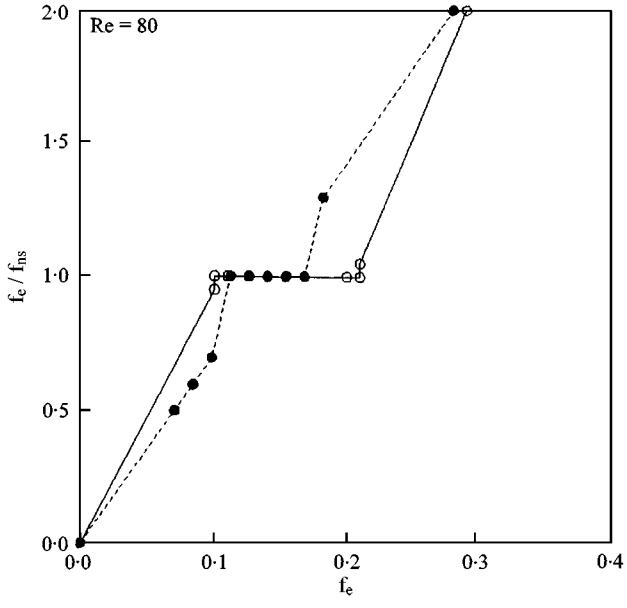

Figure 6. A comparison of frequency range for $Re = 80$. ○-○-○- Tanida *et al.* [18]; ●-●-● Present study.

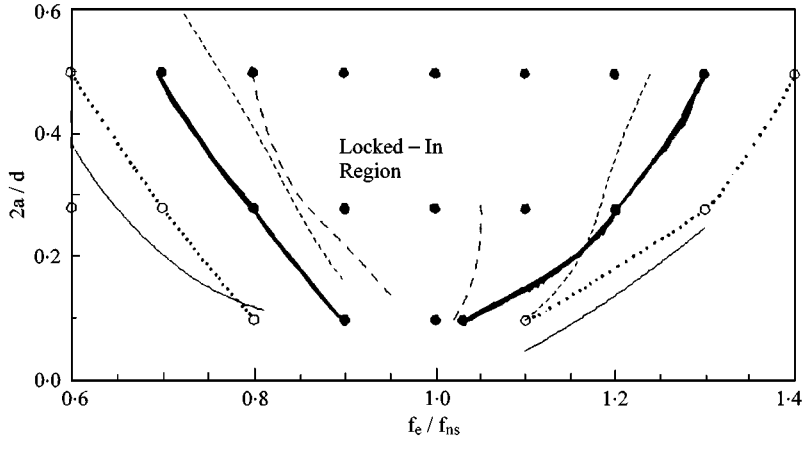

Figure 7. Comparison of the "lock-in" boundary. —— Li *et al.* [6]; $Re = 100$; - - - Koopman [4]; $Re = 100$; – – – – Mengeghini and Bearman [8]; $Re = 200$; ○···○···○ Present study (non-lock-on); $Re = 80$; ●-●-● Present study (lock-on); $Re = 80$.

together with chaotic states in the narrow regions immediately adjacent to the lock-on boundaries. These are conceptually similar to the experimental boundary given by Koopmann [4] in an overall appearance.

4.3.2. *Structure of the wake*

Streamlines indicate the flow pattern at a given instant of time, and truly represent the velocity vectors of the fluid flow domain. The sinuous motion of the

fluid flow in the wake region and its wavelength have been found to be influenced by the cylinder excitation frequency. As mentioned earlier, streamlines or the pathlines do not manifest in the spatio-temporal history of the wake and the associated convection influences. Hence, NPR is applied by the continuous release of particles, and the vortex structure under the influence of vibration is obtained. Streakline plots obtained from the present investigation imbibe the history and transport effects associated with the "phenomenon of vortex shedding" and that due to "phase locking". During "lock-on", vortices are forcibly shed at the cylinder vibration frequency, rather than at the Strouhal frequency. This interesting aspect of vortex shedding is very well captured in the streakline plots and is depicted in Figure 8. Also presented are the wake patterns, which are obtained under the influence of excitation frequency at a fixed amplitude of vibration ($a/d = 0{\cdot}14$). At lower values of this imposed excitation frquency ($f_e/f_{ns} < 0{\cdot}8$), the shedding frequency is totally uninfluenced in comparison with the pattern for the natural shedding case (Figure 8(a)). This is also observed at higher values of cylinder vibration, i.e., $f_e/f_{ns} > 1{\cdot}2$ (i.e. Figure 8(e)). When the excitation frequency is strong enough to drive the shedding frequency, the "locked-in" nature of the wake structure can be observed. When the imposed excitation frequency is less than the Strouhal frequency, i.e., for $f_e/f_{ns} < 1{\cdot}0$, and when it is able to control the vortex shedding frequency, then it results in a sparse vortex structure. However, the number of these conglomerate structures is larger, when the excitation frequency is higher than the Strouhal frequency ($f_e/f_{ns} > 1{\cdot}0$), and when it is "locked-in". Due to phase locking, concentration of vorticity involves the entire near wake and results in a tighter vortex structure as f_e/f_{ns} ratio is increased. The plot also shows a connection between various eddies by a trial streakline.

4.3.3. *Lift and drag*

The temporal variation in the lift and drag coefficient histories are presented in Figure 9. Here, a "beat" pattern in the lift history exists over the frequency range, when there is no synchronization, (i.e., for $f_e/f_{ns} = 0{\cdot}6$, $0{\cdot}7$, $1{\cdot}3$ and $1{\cdot}4$). However, a kind of highly organized behavior is observed over the "lock-in" frequency range ($f_e/f_{ns} = 0{\cdot}8$–$1{\cdot}2$), which has also indicated the existence of a unified and single dominant frequency in the FFT plots in Figure 5. The lift coeffficient histories are useful in obtaining the vortex shedding frequency, and hence the Strouhal numbers. Mean drag values are obtained from the temporal histories of the drag coefficients. For $Re = 80$, the mean drag amplification can be noticed over the "lock-in" range. This is compared with the available experimental results of Tanida *et al.* [18] in Figure 10(a). Here, when the excitation frequency is in the neighborhood of the Strouhal frequency, a marked increase in the mean drag values can be observed. However, the experimentally predicted peak is sharper than the present simulation. The Reynolds number dependency on the variation of mean drag values, against an imposed excitation frequency, is presented in Figure 10(b). During "lock-on", the drag peak predicted for $Re = 144$ is higher when compared to $Re = 80$. However, when there is no phase locking, the drag values are almost equivalent to their corresponding natural shedding drag values.

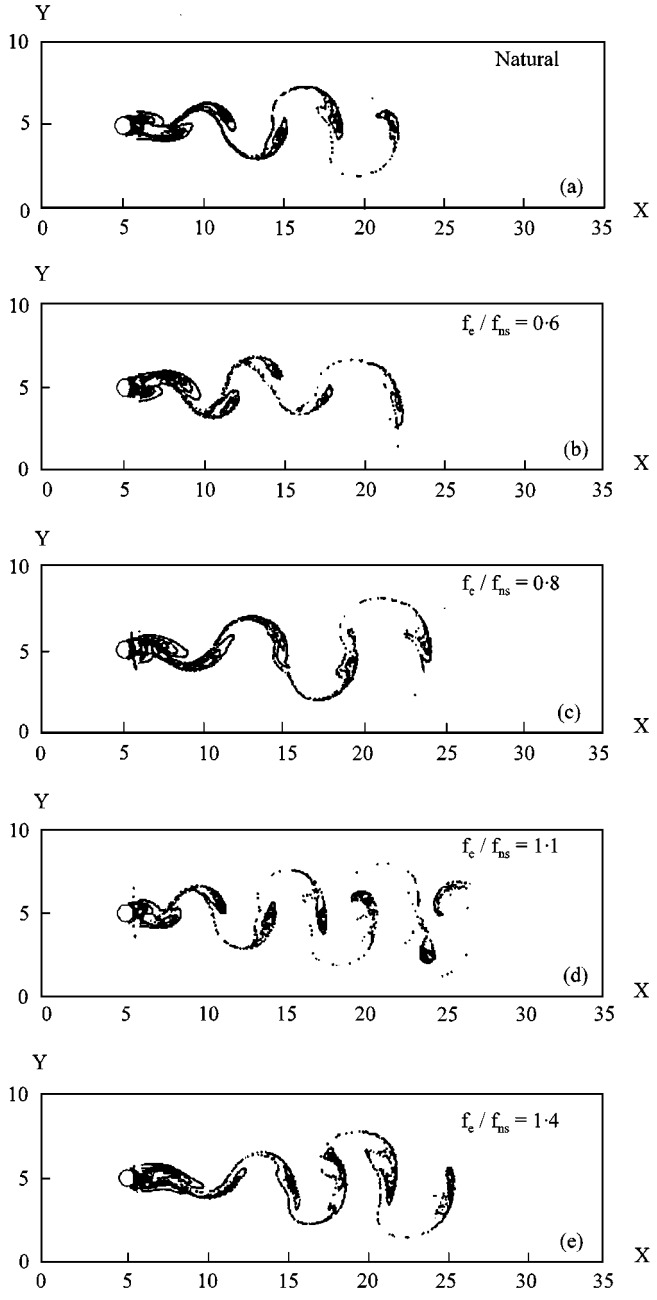

Figure 8. Wake structures under the influence of cylinder vibration.

5. SUMMARY AND CONCLUSIONS

Laminar flow past a transversely vibrating circular cylinder is numerically simulated by a modified velocity correction method. A Galerkin-weighted residual finite element formulation is employed for spatial discretization along with

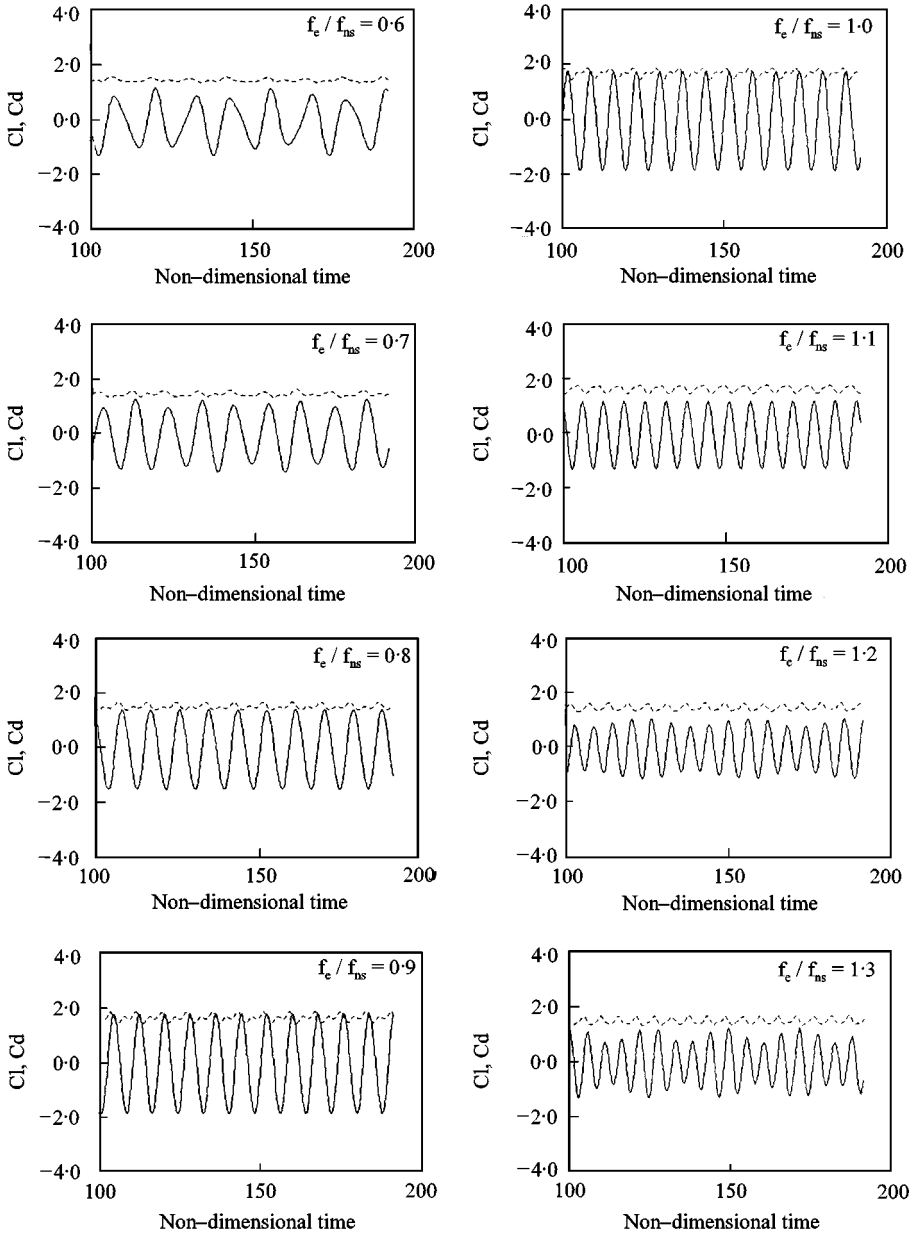

Figure 9. Temporal variations in lift and drag coefficients: —— C_l; --- C_d.

a second-order Runge–Kutta (R–K) time integration. The method of numerical particle release (NPR) is incorporated. The frame of reference is fixed with respect to the vibrating cylinder. An additional acceleration term, which arises out of this non-inertial transformation, is added to the Y-momentum equation. An analysis of the phase plane and the FFTs reveal the influence of varying excitation frequencies and the amplitude of vibration on the downstream wake structure. A good

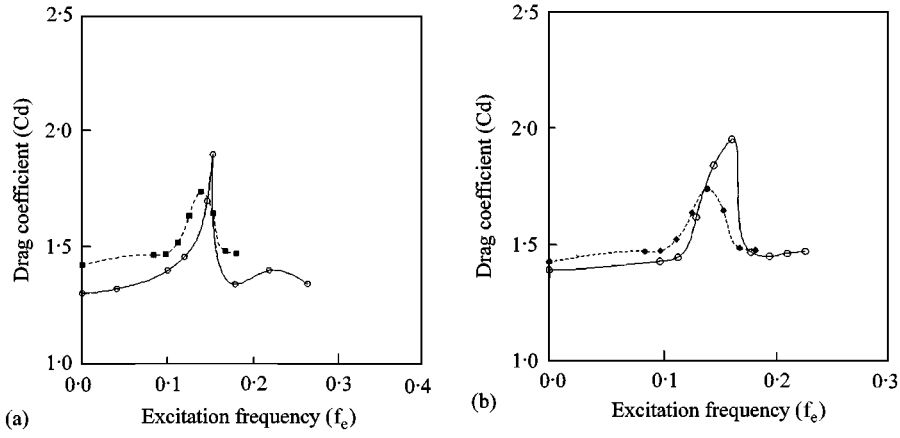

Figure 10. (a) Comparison of drag amplification for $Re = 80$. ○-○-○ Tanida *et al.* [18]; ●-●-● present study. (b) Mean drag variation with excitation frequency. ●●●●● $Re = 80$; ○○○○ $Re = 144$.

agreement with the available experimental and numerical investigations is achieved. Findings of the present simulation can be outlined as follows:

- For certain amplitudes of vibration and frequency combinations, vortices are forcibly shed at the cylinder vibration frequency rather than at the shedding frequency (lock-on).
- The influence of "phase-lock-on" is clearly depicted in the form of wake structures, phase plane plots, FFTs, temporal lift and drag coefficients, etc.
- In the phase plane, a "limit-cycle" results during "lock-on", while the phase plane plot is irregular, aperiodic and chaotic under "non-lock-on".
- Under the influence of phase locking, vortex street is expanded at lower frequencies of vibration, while it is compressed at higher frequencies. Vorticity concentration results in a tighter and a sparse vortex structure at higher and lower frequencies of cylinder vibration respectively.
- In the streakline plots, eddies are always connected by a trail streakline, which is also the case for natural vortex shedding.
- Drag amplification is successfully predicted, when the imposed excitation frequency is in the neighborhood of the Strouhal frequency.

REFERENCES

1. B. E. Eaton 1987 *Journal of Fluid Mechanics* **180**, 117–145. Analysis of laminar vortex shedding behind a circular cylinder by computer-aided flow visualization.
2. R. Chilukuri 1987 *ASME Transactions Journal of Fluids Engineering* **109**, 166–171. Incompressible laminar flow past a trasversely vibrating cylinder.

3. R. E. D. Bishop and A. Y. Hassan 1964 *Proceedings of the Royal Society of London, Series A* **277**, 51–75. The lift and drag forces on a circular cylinder oscillating in a flowing fluid.
4. G. H. Koopman 1967 *Journal of Fluid Mechanics* **28**, 501–512 The vortex wakes of vibrating cylinders at low Reynolds numbers.
5. S. E. Hurlbut, M. L. Spaulding and F. M. White 1982 *Transactions of the ASME Journal of Fluids Engineering* **104**, 214–222. Numerical simulation for laminar two-dimensional flow past a cylinder oscillating in a uniform stream.
6. J. Li, J. Sun and B. Roux 1992 *Journal of Fluid Mechanics* **237**, 457–478. Numerical study of an oscillating cylinder in uniform flow and in the wake of an upstream cylinder.
7. J. Sun, J. Li and B. Roux 1993 *International Journal for Numerical Methods in Fluids* **16**, 915–929. Flow regimes and frequency selection of a cylinder oscillating in an upstream cylinder wake.
8. J. R. Meneghini and P. W. Bearman 1995 *Journal of Fluids and Structures* **9**, 435–455. Numerical simulation of high amplitude oscillatory flow about a circular cylinder.
9. R. Wei, A. Sekine and M. Shimura 1995 *International Journal for Numerical Methods in Fluids* **21**, 993–1005. Numerical analysis of 2D vortex-induced oscillations of a circular cylinder.
10. G. Ren and T. Utnes 1993 *International Journal for Numerical Methods in Fluids* **17**, 349–364. A finite element solution of the time dependent incompressible Navier–Stokes equations using a modified velocity correction method.
11. A. J. Chorin 1966 *Journal of Computational Physics* **2**, 12–26. A numerical method for solving incompressible viscous flow problems.
12. C. A. J. Fletcher 1984 *Computational Galerkin Methods*. New York, U.S.A.: Springer.
13. L. J. Segarlind 1984 *Applied Finite Element Analysis*. New York, U.S.A.: Wiley.
14. B. S. V. Patnaik 1998 *Ph.D. Thesis, IIT, Madras, India*. Finite element analysis of flow past a circular cylinder and two cylinders in tandem: influence of vibration, buoyancy.
15. B. S. V. Patnaik, K. N. Seetharamu and P. A. Aswatha Narayana 1996 *International Journal of Numerical Methods for Heat and Fluid Flow* **6**, 65–81. Simulation of laminar confined flow past a circular cylinder with integral wake splitter involving heat transfer.
16. Visualized Flow 1988 *Fluid Motion in Basic Engineering Situations Revealed by Flow Visualization*, Complied by Japanese Society of Mechanical Engineers, Tokyo: Pergamon Press.
17. A. E. Perry, M. S. Chong and T. J. Lim 1982 *Journal of Fluid Mechanics* **116**, 77–90. The vortex shedding process behind two dimensional bluff bodies.
18. Y. Tanida, A. Okajima and Y. Watanabe 1973 *Journal of Fluid Mechanics* **61**, 769–784. Stability of a circular cylinder oscillating in uniform flow and in a wake.
19. G. M. Karniadakis and G. S. Triantafyllou 1989 *Journal of Fluid Mechanics* **199**, 441–469. Frequency selection and asymptotic states in laminar wakes.
20. G. M. Karniadakis 1988 *International Journal of Heat and Mass Transfer* **31**, 107–118. Numerical simulation of forced convection heat transfer from a cylinder in cross flow.
21. C. H. K. Williamson 1988 *Physics of Fluids* **31**, 2742–2744. Defining a universal and continuous Strouhal relationship for the laminar vortex shedding of a circular cylinder.
22. J. Y. Sa and K. S. Chang 1991 *International Journal for Numerical Methods in Fluids* **12**, 463–474. Shedding patterns of near wake vortices behind a circular cylinder.
23. L. S. G. Kovasznay 1949 *Proceedings of Royal Society Series A* **198**, 174–190. Hot wire investigation of the wake behind cylinders at low Reynolds numbers.
24. O. M. Griffin and C. W. Votaw 1972 *Journal of Fluid Mechanics* **51**, 31–48. The vortex street in the wake of a vibrating cylinder.